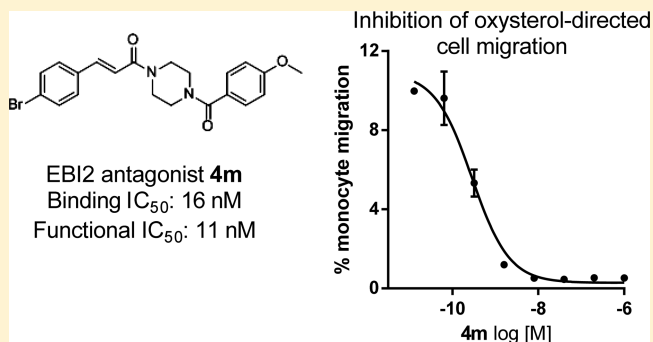


Identification and Characterization of Small Molecule Modulators of the Epstein–Barr Virus-Induced Gene 2 (EBI2) Receptor

Francois Gessier,[†] Inga Preuss,[‡] Hong Yin,^{||} Mette M. Rosenkilde,[⊥] Stephane Laurent,[‡] Ralf Endres,[§] Yu A. Chen,^{||,∇} Thomas H. Marsilje,^{||} Klaus Seuwen,[‡] Deborah G. Nguyen,^{||,#} and Andreas W. Sailer^{*,‡}[†]Global Discovery Chemistry; [‡]Developmental & Molecular Pathways, [§]Analytical Sciences, Novartis Institutes for BioMedical Research, Basel 4002, Switzerland^{||}Genomics Institute of the Novartis Research Foundation (GNF), San Diego, California 92121, United States[⊥]Laboratory for Molecular Pharmacology, Department of Neuroscience and Pharmacology, Faculty of Health and Medical Sciences, University of Copenhagen, Copenhagen 2200, Denmark

Supporting Information

ABSTRACT: Oxysterols have recently been identified as natural ligands for a G protein-coupled receptor called EBI2 (aka GPR183) (*Nature* **2011**, 475, 524; 519). EBI2 is highly expressed in immune cells (*J. Biol. Chem.* **2006**, 281, 13199), and its activation has been shown to be critical for the adaptive immune response and has been genetically linked to autoimmune diseases such as type I diabetes (*Nature* **2010**, 467, 460). Here we describe the isolation of a potent small molecule antagonist for the EBI2 receptor. First, we identified a small molecule agonist NIBRS1 (**1**), which enabled identification of inhibitors of receptor activation. One antagonist called NIBR127 (**2**) was used as a starting point for a medicinal chemistry campaign, which yielded NIBR189 (**4m**). This compound was extensively characterized in binding and various functional signaling assays. Furthermore, we have used **4m** to block migration of a monocyte cell line called U937, suggesting a functional role of the oxysterol/EBI2 pathway in these immune cells.



INTRODUCTION

Oxysterols are oxidized metabolites of cholesterol which have been linked to many fundamental physiological processes. They are key regulators in sterol and fat metabolism and are metabolic intermediates in the synthesis of bile acids from cholesterol and have been shown to interact with a wide variety of proteins. First and foremost, binding of oxysterol to the insulin-induced gene 1 (INSIG1) with a subsequent block of sterol regulatory element-binding protein (SREBP) mediates gene transcription and coordinates cholesterol biosynthesis.^{5,6} Second, several nuclear hormone receptors have been shown to interact with oxysterols and in part use them as natural ligands. Those include the liver x receptor (LXR)^{7,8} and the two retinoid related orphan receptors ROR α and ROR γ .^{8–10} Oxysterol-binding proteins (OSBP) are another class of lipid-binding proteins that are conserved from yeast to humans and have been implicated in sterol transport and regulators of protein complex assembly (for a review, see ref 11). Furthermore, oxysterols can also function as molecular chaperons as demonstrated by their interaction with the Niemann–Pick type C1 (NPC1) protein, an endosomal membrane protein required for cholesterol efflux.¹² In addition to the interaction with this diverse range of biological

regulators, modulation of signaling pathways governed by G protein-coupled receptors (GPCR) have recently become apparent. Activation of the hedgehog pathway through direct allosteric interaction of 20-hydroxycholesterol with Smoothened, a seven transmembrane receptor, regulates this critical pathway in development and cancer.^{13–15} We and others^{1,2} have identified 7 α ,25-dihydroxycholesterol (7 α ,25-OHC) and closely related compounds as natural ligands of the EBI2 receptor. In this pathway, oxysterol not only activates receptor signaling but subsequently also leads to directed cell migration of the receptor expressing immune cells toward the source of oxysterol ligand production in vitro and in vivo. Especially for activated B cells, this chemoattraction system was shown to be critically involved in positioning cells at distinct locations within the germinal center reaction.^{1,16}

To further delineate the physiological role of EBI2, there is a need for pharmacological tools which can modulate receptor function. As of today, no small molecule agonist has been described for EBI2 and there are only two reports on an EBI2 antagonist called GSK682753A.^{17,18} This compound was

Received: December 17, 2013

Published: March 28, 2014

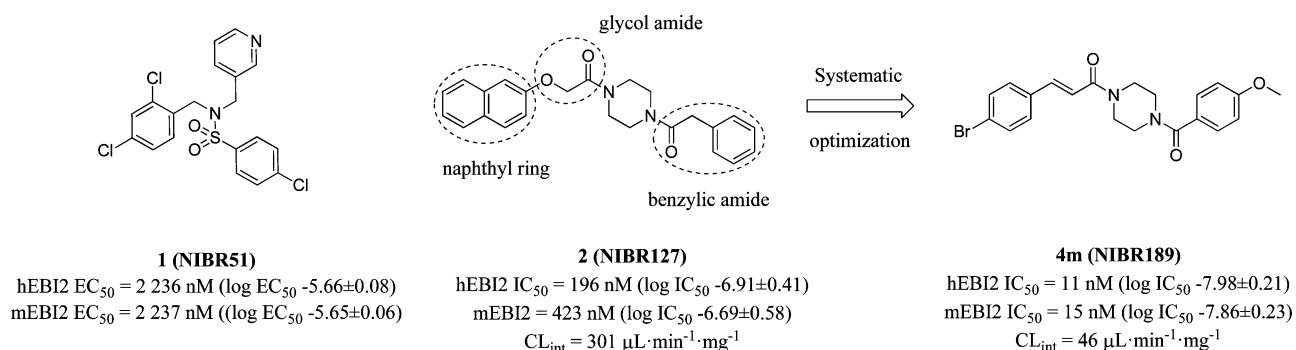


Figure 1. EBI2 small molecule agonist **1** and antagonists **2,4m**. A small molecule EBI2 agonist **1** (NIBR51) was identified by screening a chemical library. Subsequently, the agonist was used to find antagonists of receptor activation such as **2** (NIBR127). Systematic optimization of **2** yielded **4m** (NIBR189), a potent and selective EBI2 antagonist with improved pharmacokinetic properties. Half-maximal effective concentration (EC_{50}) and half-maximal inhibitory concentration (IC_{50}) values are given in nanomolar concentrations with standard deviation of the mean calculated on the logarithmic value from three or more independent experiments. Intrinsic clearance (CL_{int}) values are based on the rate and extent of metabolism of the compounds as determined in a mouse liver microsome assay by the disappearance of the parent compound from the reaction mixtures. Representative dose–response curves for all three compounds can be found in the Supporting Information (Figure S1).

identified by its ability to antagonize EBI2 constitutive activity in a recombinant system¹⁷ and was characterized by its ability to block selected second messenger systems.¹⁸ In this report, we describe identification and characterization of a small molecule agonist and detail the chemical optimization from a screening hit to **4m**, a potent and selective EBI2 antagonist with improved pharmacokinetic properties which will help to probe the physiological function of EBI2 in health and disease.

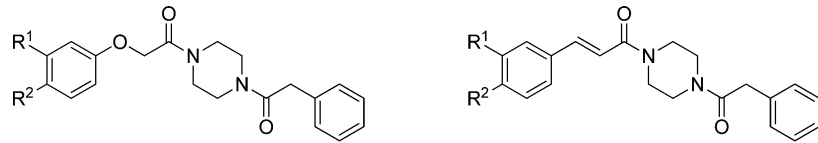
RESULTS

Prior to the isolation of oxysterols as natural ligands for EBI2,^{1,2} we searched for small molecule surrogate agonists which could be used to functionally activate the EBI2 receptor. First, we generated a Chinese hamster ovary (CHO) cell line expressing recombinant human EBI2, a promiscuous $G\alpha 16$ protein, as well as apo-aequorin. We screened a small molecule library with about 100000 compounds (100 K) using release of intracellular calcium detected by aequorin bioluminescence as primary assay readout. With this experiment, we identified **1** as an agonist for the EBI2 receptor (Figure 1) with a half-maximal concentration of activation (EC_{50}) for the human EBI2 of 1148 nM (log EC_{50} -5.94 ± 0.05, n = 2). The potency of the compound on mouse EBI2, with a 88% amino acid sequence identity to the human receptor, was confirmed in another calcium release assay (FLIPR-type; human EBI2 EC_{50} , 2236 nM (log EC_{50} -5.66 ± 0.08, n = 11); mouse EBI2 EC_{50} , 2237 nM (log EC_{50} -5.65 ± 0.06, n = 11)). The amino acid identity between the human and mouse EBI2 is 88%. Specificity of receptor activation was tested in an orthogonal assay format using a β -arrestin interaction based Pathhunter platform^{19,20} with albeit weaker activity (EC_{50} , 6050 nM (log EC_{50} -5.23 ± 0.13, n = 2)). In this assay format, a β -galactosidase enzyme is split into two parts. While one part is fused C-terminally to the EBI2 receptor, the other part is attached to the β -arrestin. Ligand activation of the receptor is followed by phosphorylation of the C-terminal part of EBI2, which subsequently leads to the attraction of β -arrestin. Proximity of the receptor and β -arrestin complements the β -galactosidase enzyme, which can be detected by conversion of the appropriate substrate. Availability of this surrogate ligand enabled the rescreen of the 100 K small molecule library for compounds which can block receptor activation by **1**. One of the identified hits was **2**, which demonstrated high affinity in the radioligand binding assay

(human EBI2 IC_{50} , 83 nM (log IC_{50} -7.13 ± 0.23, n = 12)) and good potency in a functional calcium release assays (human EBI2 IC_{50} , 196 nM (log IC_{50} -6.91 ± 0.41, n = 23)) and is active at the mouse receptor (mouse EBI2 FLIPR IC_{50} , 423 nM (log IC_{50} -6.69 ± 0.58, n = 31)). Furthermore, testing of **2** against the human CysLTR2, one of the most closely related GPCRs to EBI2, did not show any inhibition to the maximal tested concentration of 10 μM (data not shown). Nevertheless, the in vitro analysis of **2**'s properties revealed a significant metabolic stability issue in mouse liver microsomes (CL_{int} = 301 $\mu\text{L}\cdot\text{min}^{-1}\cdot\text{mg}^{-1}$), which limited the utility of this compound to support our planned in vivo experiments. Our concern was not only the high intrinsic microsomal clearance of **2**, which negatively impacts the pharmacokinetic profile of the compound, but also the potential formation of active metabolites, which makes the interpretation of any biological observations much more difficult and complex. Moreover, as our tool compound should also be deployed to in vivo mouse models, increased potency on the mouse EBI2 receptor was desired. Thus, we initiated a medicinal chemistry effort aimed to quickly optimize **2** and identify a compound with an adequate PK profile after intravenous administration by improving the metabolic stability while increasing the potency especially on the mouse receptor and maintaining selectivity.

In the absence of structural information about EBI2 and experimental determination of the metabolic weak spots of **2** that would have been useful to guide our optimization, we opted for a systematic and broad evaluation of the left-hand side (LFS) naphthyl ring, the glycolamide core and the right-hand side (RHS) benzylic amide of **2**. These efforts led to the discovery of compound **4m** as disclosed in this paper (Figure 1). During this study, all new derivatives were tested on the human and the mouse EBI2 receptors (FLIPR-type calcium release: IC_{50}), and the most potent antagonists were assayed in a mouse liver microsomes assay to determine their CYP metabolic stability (clearance CL_{int}).

The optimization of **2** started with the RHS naphthyl ring, known to be readily metabolized in vivo toward different oxidative pathways and, therefore, considered to likely play a major role in the high metabolic clearance of **2**. The naphthyl ring was replaced first by the corresponding quinolines in order to block potential metabolic weak spots and reduce the electronic density of the aromatic system, making it less prone

Table 1. Impact of the LHS Optimization of **2** on the Inhibition of the Mouse and the Human EB12 Receptors (FLIPR-Type Assay) and on the Metabolic Stability (Mouse Liver Microsomes Assay)^a


compd	glycolamide series 2		cinnamyl series 3		CL _{int} (μL·min ⁻¹ ·mg ⁻¹) ^c
	R ¹	R ²	human EB12 IC ₅₀ (nM) (log IC ₅₀ ± SD) ^b	mouse EB12 IC ₅₀ (nM) (log IC ₅₀ ± SD) ^b	
2	–benzene–		196 (–6.91 ± 0.41)	423 (–6.69 ± 0.58)	301
2a	H	Cl	330 (–6.51 ± 0.18)	979 (–6.01 ± 0.06)	107
2b*	H	Br	28 (–7.55)	100 (–7.00)	131
2c*	Me	Me	2934 (–5.53)	4341 (–5.36)	
3a*	H	Br	21 (–7.68)	29 (–7.54)	107
3b*	H	Me	19 (–7.72)	92 (–7.04)	447
3c*	H	OMe	29 (–7.54)	207 (–6.68)	113
3d*	Cl	Cl	24 (–7.62)	44 (–7.36)	
3e*	F	Me	17 (–7.77)	46 (–7.34)	

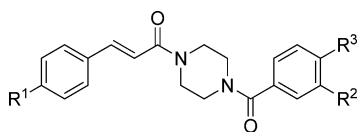
^aReceptor binding data for all compounds using a [³H] 7 α ,25-OHC radioligand binding assay can be found in the Supporting Information (Table S2). ^bIC₅₀ were determined in a calcium release assay (FLIPR-type) with duplicate values in 8-point dose titrations. Values are given with standard deviation of the mean (SD) from at least two independent experiments. Compounds with * were determined in screening mode with duplicate values in a single dose titration. ^cIntrinsic clearance (CL_{int}) values are based on the rate and extent of metabolism of the compounds as determined in a mouse liver microsome assay by the disappearance of the parent compound from the reaction mixture.

to oxidation. We also speculated that well positioned nitrogens could potentially induce additional interaction with EB12 leading to a gain in potency. Unfortunately, all compounds made along this line did not show improved activity at the highest tested concentration of 10 μM, suggesting that the naphthyl moiety binds into a hydrophobic region of EB12 with a preference of lipophilic residues. As an alternative, we decided to mimic the naphthyl moiety by various meta- and para-substituted phenyl rings. On the basis of our previous observation, we performed a systematic screen of both aryl positions focused on lipophilic residues such as halogens, alkyls or methoxy. While all meta-substituted derivatives were found completely inactive (IC₅₀ >10 μM) on both human and mouse EB12, the para-substitution of the phenyl proved to be a successful alternative to replace the naphthyl ring. Even there, a very restricted number of substituents were tolerated and from all compounds made, and only the 4-bromo analogue **2b** led to a gain of potency of about 7-fold compared to **2** (Table 1). Even the 3,4-dimethyl analogue **2c**, which was expected to better mimic the naphthyl ring, led to a decreased EB12 antagonism. Therefore, we concluded that the LHS region of **2** binds most likely in a hydrophobic pocket of EB12 and adequate hydrophobic contacts within this pocket are essential for potency. Finally, the metabolic stability of compound **2a** was assessed and, as expected, revealed a significant reduction of the metabolic clearance in our in vitro assay (CL_{int} = 107 μL·min⁻¹·mg⁻¹) but still remained in the medium range.

To further expand SAR in the core of the scaffold, we investigated the glycolamide function of compound **2b** and replaced it by a cinnamyl function. The corresponding analogue **3a** showed similar activity on the human EB12 receptor (IC₅₀ = 21 nM (log IC₅₀ –7.68, *n* = 1)), whereas the potency at the mouse receptor (IC₅₀ = 29 nM (log IC₅₀ –7.54, *n* = 1)) surprisingly increased (Table 1). To verify if the cinnamyl function did not alter the LHS structure–activity relationship (SAR), we rapidly reinvestigated the phenyl moiety and prepared various monosubstituted phenyl analogues. While

the observed SAR was very similar to the glycolamide series with a pronounced preference for the para-substitution pattern, it appeared that the range of tolerated substituents was not limited to the unique bromine or chlorine anymore but could be extended to several others, as illustrated with the 4-methyl and 4-methoxy analogues **3b** and **3c**. Moreover, the 3,4-disubstitution was well tolerated in the cinnamyl series, leading to potent analogues on both human and mouse receptors such as **3d** and **3e**. On the basis of these findings, we hypothesized that the cinnamyl linker induced a slightly different positioning of the LHS phenyl moiety into the EB12 binding pocket, consequently allowing the pocket to accommodate a broader range of substituents with improved hydrophobic contacts, leading to more potent antagonism. Finally, we investigated the metabolic stability of some of the new potent analogues but did not observe any improvement compared to **2a**.

Because of structural constraints in the LHS region of **2**, only a small number of potent compounds could be identified with only limited improvement in metabolic stability. Thus, in the next step we focused on the optimization of the RHS benzyl amide of compound **3c**. Encouraged by a flexible chemical space and easily accessible compounds for library production, we systematically screened the aromatic ring of the benzyl amide moiety. All positions of the aromatic ring of the benzyl amide moiety were substituted by various small hydrophobic, H-bond acceptor and H-bond donor residues. Disappointingly, the obtained compounds led to a significant loss of activity toward EB12 and the parent compound **3c** remained the most potent analogue within the series. In a second round of optimization, we moved from benzylic amides to aryl amides and reinvestigated each positions of the phenyl ring. Ortho and meta substitutions were found detrimental for potency, with the exception of the 3-methyl analogue **4a**, which was equipotent to **3c** against the human EB12 receptor (IC₅₀ = 31 nM (log IC₅₀ –7.53 ± 0.13, *n* = 2)) and slightly more active on the mouse receptor (IC₅₀ = 84 nM (log IC₅₀ –7.15 ± 0.36, *n* = 2)) (Table 2). In contrast, the para-position appeared to be much more

Table 2. Impact of the RHS Optimization of 3c on the Inhibition of the Human and the Mouse EBI2 Receptors (FLIPR-Type Assay) and on the Metabolic Stability (Mouse Liver Microsomes Assay)^a

compd	R ¹	R ²	R ³	human EBI2 IC ₅₀ (nM) (log IC ₅₀ ± SD) ^b	mouse EBI2 IC ₅₀ (nM) (log IC ₅₀ ± SD) ^b	CL _{int} (μL·min ⁻¹ ·mg ⁻¹) ^c
4a	OMe	Me	H	31 (-7.53 ± 0.13)	84 (-7.15 ± 0.36)	
4b*	OMe	H	CF ₃	98 (-7.01)	81 (-7.09)	295
4c	OMe	H	Br	71 (-7.17 ± 0.18)	92 (-7.10 ± 0.34)	
4d	OMe	H	Me	40 (-7.40 ± 0.09)	65 (-7.27 ± 0.39)	231
4e*	OMe	H	OMe	32 (-7.49)	55 (-7.26)	90
4f*	OMe	H	NMe ₂	19 (-7.72)	20 (-7.70)	
4g*	OMe	H	CO ₂ Me	17 (-7.77)	18 (-7.74)	
4h*	OMe	-CH ₂ CH ₂ O-		18 (-7.74)	29 (-7.54)	87
4i*	OMe	Me	Cl	13 (-7.89)	21 (-7.68)	239
4j*	OMe	Me	Me	44 (-7.36)	52 (-7.28)	
4k*	Cl	-CH ₂ CH ₂ O-		16 (-7.80)	23 (-7.64)	60
4l*	Br	-CH ₂ CH ₂ O-		5 (-8.30)	6 (-8.22)	73
4m	Br	H	OMe	11 (-7.98 ± 0.21)	15 (-7.86 ± 0.23)	46

^aReceptor binding data for all compounds using a [³H] 7α,25-OHC radioligand binding assay can be found in the Supporting Information (Table S3). ^bIC₅₀ were determined in a calcium release assay (FLIPR-type) with duplicate values in 8-point dose titrations. Values are given with standard deviation of the mean (SD) from at least two independent experiments. Compounds with * were determined in screening mode with duplicate values in a single dose titration. ^cIntrinsic clearance (CL_{int}) values are based on the rate and extent of metabolism of the compounds as determined in a mouse liver microsome assay by the disappearance of the parent compound from the reaction mixture.

Table 3. Intravenous (iv) and Oral (po) Pharmacokinetics Parameters of Compounds 4e and 4m in Mice^a

compd	dose (mg·kg ⁻¹)	CL (μL·min ⁻¹ ·mg ⁻¹)	t _{1/2} (h)	V _{ss} (L·kg ⁻¹)	AUC (nmol·h·L ⁻¹)	C _{max} (nmol·L ⁻¹)	t _{max} (h)	F (%)
4e iv	1	52	0.2	0.8	841			
4m iv	1	16	1.1	1.4	2 435			
4m po	3				3 608	835	1	49

^aPharmacokinetic parameters were calculated from blood levels after iv (1 mg·kg⁻¹) and po (3 mg·kg⁻¹) administration to conscious mice (cassette dosing experiments with six compounds in maximum). Shown are composite parameters from sparse sampling. Species/strain: male mice (C57BL/6). Formulation iv solution in NMP: Plasma (10:90), administration volume 5 mL·kg⁻¹. Formulation po suspension in Tween 80: CMC05 (0.5:99.5), administration volume 10 mL·kg⁻¹. CL, total blood clearance. t_{1/2}, terminal blood half-life. V_{ss}, apparent volume of distribution at steady state. AUC, area under the concentration–time curve (extrapolated to infinity). C_{max}, maximal blood concentration after po administration. T_{max}, time of peak blood concentration after po administration. F (%), oral bioavailability.

attractive and flexible for substitution. Different types of substituents resulted in improved potency compared to compound 3c with a preference for polar (compounds 4e–g) over lipophilic (compounds 4b–d) residues. This is illustrated by the high activity of the 4-dimethylamino and the 4-methylester analogues 4f and 4g. While the para position of the RHS phenyl ring accommodated a broader range of substituents, their relative sizes appeared crucial for potency. In fact, larger substituents such as heterocycles, cycloalkyls, or aryls were found weaker or inactive on both mouse and human EBI2 receptors. To further expand the SAR, we finally synthesized different 3,4-disubstituted or bicyclic derivatives by combining some of our preferred meta- and para-substituents. All compounds made with this design motif demonstrated a synergy between the different substituents, leading overall to improved activity toward EBI2 compared to their corresponding monosubstituted analogues (e.g., analogues 4h–j in Table 2). In summary, the optimization of the benzylic amide of compound 3c delivered a set of potent compounds with a good level of substituent diversity. Selected compounds were tested in our in vitro metabolic clearance assay, and we found that the nature of the substituent of the aryl amide tail plays a significant role on the overall metabolic stability of our

compounds. Indeed, the compounds bearing lipophilic residues such as 4b, 4d, and 4i were highly metabolized independently from the electron withdrawing or donating properties of the substituent. In contrast, compounds substituted with polar residues such as 4e and 4h were found to be more stable toward metabolic degradation while the intrinsic clearance remained in the medium range. Being particularly interested in the in vivo clearance properties of our compounds, we conducted a rodent PK study of the most promising derivatives by intravenous administration in mice. In all cases, we observed medium to low in vivo blood clearances which were consistent with the measured in vitro data. Of all the compounds tested, 4e showed the best PK profile (Table 3).

To follow up on these results, in a final step we synthesized another library of compounds within the cinnamyl series by combining our best LHS and RHS residues. These were selected based on their intrinsic potency on human and mouse EBI2 and their positive impact on metabolic stability. As exemplified by compounds 4k, 4l, and especially 4m (Table 2), with this approach we were able to generate a set of potent EBI2 antagonists with similar affinities for the human and the mouse receptor and overall improved metabolic stability properties compared to compound 4e. To confirm the

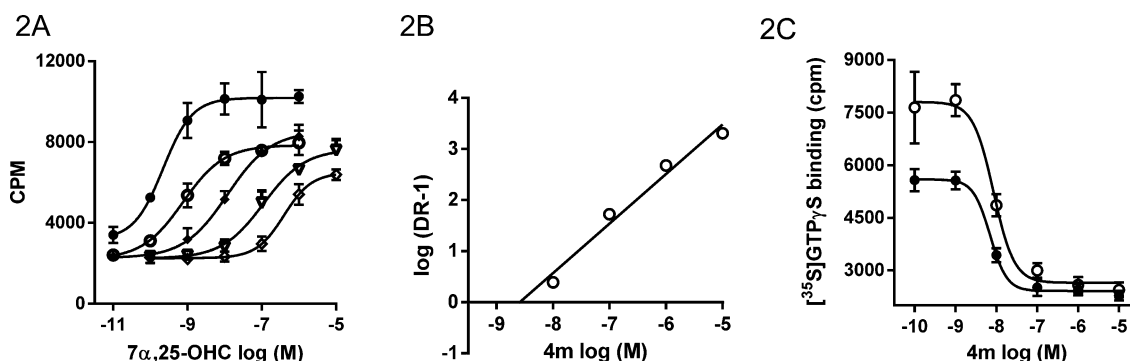


Figure 2. Pharmacological characterization of **4m** by $[^35\text{S}]\text{GTP}\gamma\text{S}$ binding in CHO cells. (A) Dose titrations of $7\alpha,25\text{-OHC}$ at fixed concentrations of **4m**. No antagonist (\bullet), or **4m** at 10 nM (\circ), 100 nM (\blacklozenge), 1000 nM (∇), 10000 nM (\diamond). (B) Schild plot analysis for **4m**. The compound displays competitive antagonism with a Hill coefficient of 1. The intersection of the X-axis is at $K_a = -8.6$. (C) Dose response of **4m** at fixed, submaximal concentrations of $7\alpha,25\text{-OHC}$ (0.33 nM (\circ), 0.1 nM (\bullet)).

observed in vitro data, we carried out a full PK evaluation of compound **4m** in mice by intravenous (iv) and oral (po) administration and found that **4m** showed a significantly lower total blood clearance than **4e** (Table 3), leading to an increased half-life and a significantly higher exposure. Moreover, on the basis of the good oral bioavailability observed for **4m**, oral administration of the compound could also be considered as an attractive alternative route for in vivo delivery. Testing of **4m** against a panel of other GPCRs, transporters, and enzymes (see Experimental Methods section for details) did not show any activity at the maximal tested concentration of 30 μM . The good mouse PK and selectivity profiles of **4m**, associated with high potency on EB12, suggests that **4m** is a suitable candidate to support in vivo activities and for the pharmacological validation of EB12.

Pharmacological Characterization of 4m. While the optimization of **4m** was guided by functional assays measuring release of intracellular calcium upon activation, we extended the characterization the pharmacological properties of **4m** by $[^35\text{S}]\text{GTP}\gamma\text{S}$ binding assays including a Schild plot analysis. First we carried out dose titrations of $7\alpha,25\text{-OHC}$ at fixed concentrations of **4m** (Figure 2A). **4m** displays competitive antagonism, and the Schild plot reveals a Hill coefficient of 1 (Figure 2B). The intersection of the X-axis corresponding to the K_a value is at -8.6 . Besides the dose-dependent right shift in the $7\alpha,25\text{-OHC}$ activation curves, the presence of **4m** also resulted in a downward shift of the activation curves. This inhibition of the basal activity of EB12 without addition of $7\alpha,25\text{-OHC}$ indicates that the antagonist also act as an inverse agonist. We also conducted dose titrations of **4m** at fixed, submaximal concentrations of oxysterol (0.33, 0.1 nM) and found IC_{50} s at 8.5 and 7.0 nM ($\log \text{IC}_{50}$ s at -8.07 ± 0.07 and -8.15 ± 0.11), respectively.

While all assays described so far were conducted with cells expressing recombinant EB12 receptors, we extended our analysis of **4m** also to immune cells expressing endogenous EB12 receptor. Screening of EB12 mRNA expression levels in several cell lines suggested that the monocyte-derived U937 cell expresses functional EB12 levels. This was confirmed by demonstrating $7\alpha,25\text{-OHC}$ dependent release of intracellular calcium with either the natural ligand $7\alpha,25\text{-OHC}$ or the small molecule activator **1** with half-maximal concentrations of activation of 14 nM ($\log \text{EC}_{50} -7.95 \pm 0.33$, $n = 5$) or 6662 nM ($\log \text{EC}_{50} -5.18 \pm 0.07$, $n = 4$), respectively (Figure 3A). **4m** and **2** can block oxysterol-dependent activation with an

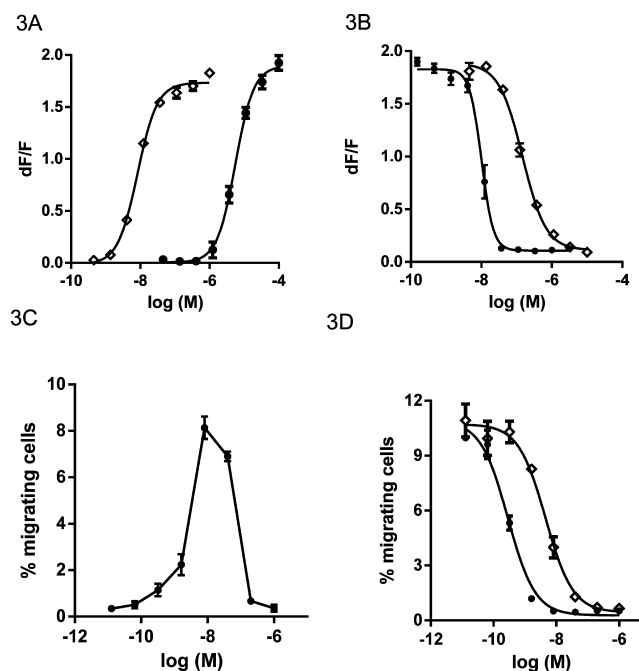


Figure 3. Pharmacological characterization of oxysterol-dependent calcium release and cell migration of U937 cells. (A) $7\alpha,25\text{-OHC}$ -dependent release of intracellular calcium in U937 cells; $7\alpha,25\text{-OHC}$ (\diamond); **1** (\bullet). (B) Block of $7\alpha,25\text{-OHC}$ -induced calcium release in U937 cells; **4m** (\bullet); **2** (∇). The $7\alpha,25\text{-OHC}$ agonist concentration used in this experiment was 100 nM. (C) $7\alpha,25\text{-OHC}$ -dependent migration of U937 cells; $7\alpha,25\text{-OHC}$ (\bullet). (D) Inhibition of $7\alpha,25\text{-OHC}$ -dependent cell migration of U937 cells by **4m** (\bullet) or **2** (∇). The $7\alpha,25\text{-OHC}$ agonist concentration used in this experiment was 20 nM. (D) All experiments were replicated three or more times, and the graphs show data from one representative experiment.

IC_{50} of 9 nM ($\log \text{IC}_{50} -8.06 \pm 0.18$, $n = 3$) or 91 nM ($\log \text{IC}_{50} -7.08 \pm 0.22$, $n = 3$), respectively (Figure 3B). Similar to B cells or dendritic cells, this activation leads to a directed migration of U937 cells in a transwell assay. For $7\alpha,25\text{-OH}$, we find an EC_{50} of 2.42 nM ($\log \text{EC}_{50} -8.64 \pm 0.18$, $n = 4$) (Figure 3C). The EB12 antagonists **4m** and **2** can block this migration with an IC_{50} of 0.3 nM ($\log \text{IC}_{50} -9.65 \pm 0.34$, $n = 4$) and 5.3 nM ($\log \text{IC}_{50} -8.31 \pm 0.20$, $n = 4$), respectively (Figure 3D).

CONCLUSION

Here we report for the first time identification of a small molecule agonist **1** for EBI2, which was successfully used to find receptor antagonists. While the utility of one of the initial antagonist hit **2**, due to potency and pharmacokinetic profile, was limited, we conducted a medicinal chemistry campaign which yielded a potent and selective EBI2 antagonist **4m**. Pharmacological characterization suggests that **4m** is a potent and selective EBI2 antagonist with pharmacokinetic properties which should allow use for *in vitro* and *in vivo* experiments. Given the selective expression of EBI2 in immune cells, much of the initial testing was directed toward paradigms of autoimmune disorders.⁴ Our results demonstrating a functional role of the oxysterol/EBI2 pathway in monocytes suggest that exploration of the physiological role of this system should be extended beyond autoimmune disorders. This was further substantiated by a recent report²¹ that showed that chemotactic migration in THP1 cells is EBI2 dependent. Considering the substantial concentration of oxysterols in atherosclerotic lesion²² and the important role of monocyte migration for the disease pathophysiology,²³ our result should encourage testing of EBI2 antagonists in paradigms relevant for cardiovascular disease.

EXPERIMENTAL SECTION

Pharmacological Characterization of EBI2 Modulators.

Calcium Mobilization Assays. Methods on for calcium mobilization assays were published previously.¹ In brief:

FLIPR-Type Calcium Assay. Cells were seeded in black/clear bottom, poly-D-Lysine coated 384-well plates at a cell density of 10000 cells/25 μ L/well using culture medium. Cells were cultured for 24 h at 37 °C/5% CO₂. Culture medium was removed, and for cell loading, 20 μ L per well of loading buffer (Calcium-4 no wash dye, Molecular Devices) were distributed into the wells and the plates were incubated for 60 min at 37 °C in 5% CO₂. With the FLIPR pipettor, 10 μ L of the different compounds diluted in FLIPR buffer (HBSS (Gibco, no. 14065) + 20 mM HEPES (Gibco, no. 1563) + 0.1% β -cyclodextrin (Sigma-Aldrich, no. C4767)) were added to the cells, and the subsequent fluorescent changes were monitored for 3 min. Using the FLIPR software tool, two values of fluorescence calcium responses were exported: F_{\max} , the fluorescence at the peak and F_{basal} corresponding to the value prior to compound injection. From these two values, the calcium response is normalized with respect to the calcium baseline values using $dF/F = (F_{\max} - F_{\text{basal}})/F_{\text{basal}}$. The maximum dF/F is called E_{\max} .

For calcium mobilization assay of the U937 cell line the protocol had to be modified. The number of cells plated for the experiment was increased to 40000/well.

EC_{50} and IC_{50} values were determined with duplicate values in 8-point dose titrations using standard software (Prism, GraphPad Software Inc.). Values are given with the standard deviation of the mean (SD) calculated from logarithmic values from two or more independent experiments. Compounds with an * were determined in screening mode with duplicate values in a single dose titration.

Aequorin Bioluminescence-Type Calcium Assay. The cells were seeded into 384-well black clear bottom plates (Greiner Bio-one) at 10000 cells/25 μ L/well in F12 medium containing 3% FBS and incubated overnight. Coelenterazine (20 μ M final) was added into the cell plates at 25 μ L/well. The cell plates were returned to incubator for 3 h. The compounds were diluted 1:20 into an intermediate plate with Tyrode buffer (130 mM NaCl, 2 mM CaCl₂, 5 mM NaHCO₃, 5 mM KCl, 1 mM MgCl₂, 20 mM HEPES, pH 7.4). Then 12.5 μ L/well of prediluted compounds were transferred into the cell assay plate and read on LumiLux (PerkinElmer) for flash luminescence. An algorithm similar to area under curve (AUC) was created in-house to analyze the aequorin kinetic data, which was named Slope Threshold (Slope 100). The algorithm defines the beginning and the end of the luminescence

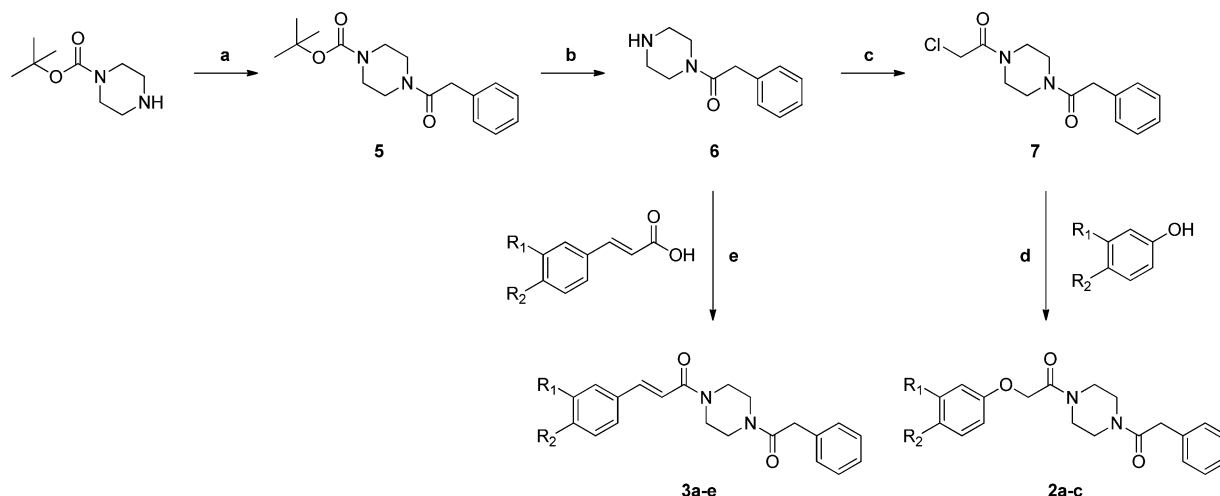
intensity peak by comparing the difference in intensity of each time point with an earlier time point and determining if the difference exceeds a defined threshold, which was usually set at 100. If it does, then the intensity of the later time point is added into the Slope Threshold's sum.

Membrane Preparation/Radioligand Binding Assay. Membranes and assays were prepared as previously described.^{1,24} In brief, CHO cells stably expressing human EBI2 were grown to confluence, washed with phosphate buffered saline (PBS) once, and frozen at -80 °C. The frozen cell pellets were resuspended in ice-cold homogenization buffer (10 mL/g, 20 mM Tris pH 7.2) supplemented with a protease inhibitor cocktail (Complete, Roche). The cell suspension was then homogenized using a Dounce homogenizer (10 strokes) with a drill. After centrifugation at 110000g for 45 min and removal of the supernatant, pellets were resuspended in sucrose buffer (50 mM Tris pH 7.2, 250 mM sucrose, 10% glycerol) by vortexing. The suspension was again homogenized using a Dounce homogenizer (10 strokes) and spun at 100000g for 45 min. The supernatant was discarded, the pellet resuspended in sucrose buffer, protein concentration determined, aliquoted, and frozen at -80 °C. These membrane preparations were used for radioligand binding as well as GTP γ S assays.

For the radioligand binding assay lyophilized wheat germ agglutinin scintillation proximity assay (SPA) beads (RPNQ0001) were purchased from GE Healthcare (Buckinghamshire, UK). One vial (500 mg) was reconstituted by adding 5 mL of distilled water to give a final concentration of 100 mg/mL. The radioligand (³H-7 α , 25-OHC) used in these experiments was batch RSE436-6 with a specific activity of 972 GBq/mmol, which was stored at -20 °C. For the assay, compounds were serially diluted into the assay buffer (HBSS (Gibco, no. 14065) + 20 mM HEPES (Gibco, no. 1563) + 0.1% β -cyclodextrin (Sigma-Aldrich, no. C4767), DMSO concentration <2%) before 10 μ L were transferred to the assay plate (Optiplate, white, flat square bottom, PerkinElmer). In a second step, 20 μ L of a membrane (10 μ g/well)/bead mixture (200 μ g/well) was added before a final addition of 20 μ L radioligand (10 nM/well). After 10 min of shaking, assay plates were incubated at room temperature overnight and then read for 1 min with a scintillation counter (Topcount, PerkinElmer). IC_{50} values were determined with using standard software (Prism, GraphPad Software Inc.).

[³⁵S]GTP γ S Binding Assay. [³⁵S]GTP γ S binding experiments were carried out as previously described.^{3,24} In brief, a volume of membrane preparation (corresponding to 20 μ g protein/well) were diluted in assay buffer (50 mM HEPES, 3 mM MgCl₂, 100 mM NaCl, 1 mM EGTA, 3 μ M GDP, 10 μ g/mL saponin, and Complete inhibitor mix, pH 7.4). [³⁵S]GTP γ S (1250 Ci/mmol, 12.5 mCi/mL) diluted in assay buffer was added to a final concentration of 1 nM and incubated 1 h at 30 °C. Subsequently, WGA PVT SPA-beads (PerkinElmer) were added (final concentration of 2.8 mg/mL), followed by 30 min of incubation at room temperature on a plate shaker. Finally, the plates were centrifuged at 1500 rpm for 5 min and the amount of radioactivity determined using a Top Count scintillation counter (Packard Instruments). The level of unspecific binding was determined by adding unlabeled GTP γ S at a final concentration of 40 μ M.

β -Arrestin Assay (Pathhunter, DiscoverRx). We applied the Pathhunter technology (DiscoverRx) to probe for an interaction of EBI2 with β -arrestin. For that, human EBI2 was cloned into the ProLink vector (DiscoverRx) for GPCR-prolink fusion protein production. Parental HEK293 cells that stably express the β -arrestin2- β -gal-EA fusion protein (HEK293-BAEA) were detached and transiently transfected with hEBI2-prolink vector using Fugene6 transfection reagent in suspension mode. Transfected cells in assay medium (Phenol Red-free DMEM with 10% FBS) were plated into white solid 384-well plates at 15000 cells/25 μ L/well. After overnight incubation, 200 nL of test molecules were transferred into the cell plates by PinTool (GNF Systems), followed by 1.5 h incubation at 37 °C, 5% CO₂. Flash detection reagents were added at 12.5 μ L/well. After a 30 min room temperature incubation, the cell plates were read on CLIPR (PerkinElmer) or Acquest (Molecular Devices) for luminescence signal. An algorithm similar to area under the curve

Scheme 1. Synthesis of Compounds 2a–c and 3a–e^a

^aReagents and conditions: (a) 2-phenylacetyl chloride, pyridine, CH₂Cl₂, RT, 1.5 h, 97%; (b) TFA, CH₂Cl₂, RT, 30 min, 80%; (c) chloroacetyl chloride, Et₃N, CH₂Cl₂, RT, 30 min, 57%; (d) K₂CO₃, DMF, RT, 16 h, 69%–89%; (e) Et₃N, HATU, DMF, RT, 3 h, 48–85%.

(AUC) was created in-house to analyze the aequorin kinetic data, which was named Slope Threshold (Slope 100). The algorithm defines the beginning and the end of the luminescence intensity peak by comparing the difference in intensity of each time point with an earlier time point, and determining if the difference exceeds a defined threshold, which was usually set at 100. If it does, then the intensity of the later time point is added into the Slope Threshold's sum.

Chemotaxis Assay for the U937 Cell Line. Prior to the migration assay, U937 cells were kept overnight in lipid-depleted media (RPMI (Gibco, no. 61870-010) + 1% NEAA (Gibco, no. 11140-035) + 1% NaPyr (Gibco, no. 11360-039) + 0.1% 2-mercaptoethanol (Gibco, no. 31350-010) + 1% Pen/Strep (Bioconcept, no. 4-01F00-H) + 10% charcoal-treated FCS (Gibco, no. 12676)). Chemotaxis was performed using HTS Transwell-96 plates with 5.0 μ m pore polycarbonate membranes (Corning, no. 3387) according to the manufacturer's protocol. In brief, lower chambers were filled with 240 μ L of compound solution in media in which the FCS was substituted with 1% BSA (Gibco, no. 15260-037), and after insertion of the filters, 0.75 \times 10⁵ cells in 75 μ L media were added to the upper chamber. After 3 h at 37 $^{\circ}$ C, cells in the lower chamber were analyzed by flow cytometry using CyFlow Space with a RobbyWell plate reader (Partec). Chemotaxis is expressed as percent of input cells.

Specificity Testing of EBI2 Antagonist 4m. To assess specificity of 4m, we have tested this compound in a panel of assays versus other GPCRs, enzymes, transporters, and other receptors. In none of these assays did we see significant interaction between these 4m and the tested receptors at concentration below 30 μ M. Binding assays included 11 different GPCRs (acetylcholine (muscarinic), M1; adenosine receptor, A2A, A3; adrenoreceptors, α 2C, β 1; cysteinyl leukotriene receptors, CysLTR1, CysLTR2; dopamine receptor, D2; histamine receptor, H1; melanocortin receptor, MC3; prostanoid receptor, TP). Transporter assays included dopamine transporter, DAT; norepinephrine transporter, NET. Enzymes included cyclooxygenase, COX-1; monoaminoxidase, MAO-A; phosphodiesterases, PDE3; PDE4D. Nuclear hormone receptor: SXR (NR112). Functional assays included three different GPCRs (5-hydroxytryptamine receptor, 5HT2A; acetylcholine receptor (muscarinic), M2; adrenoreceptor, α 1A).

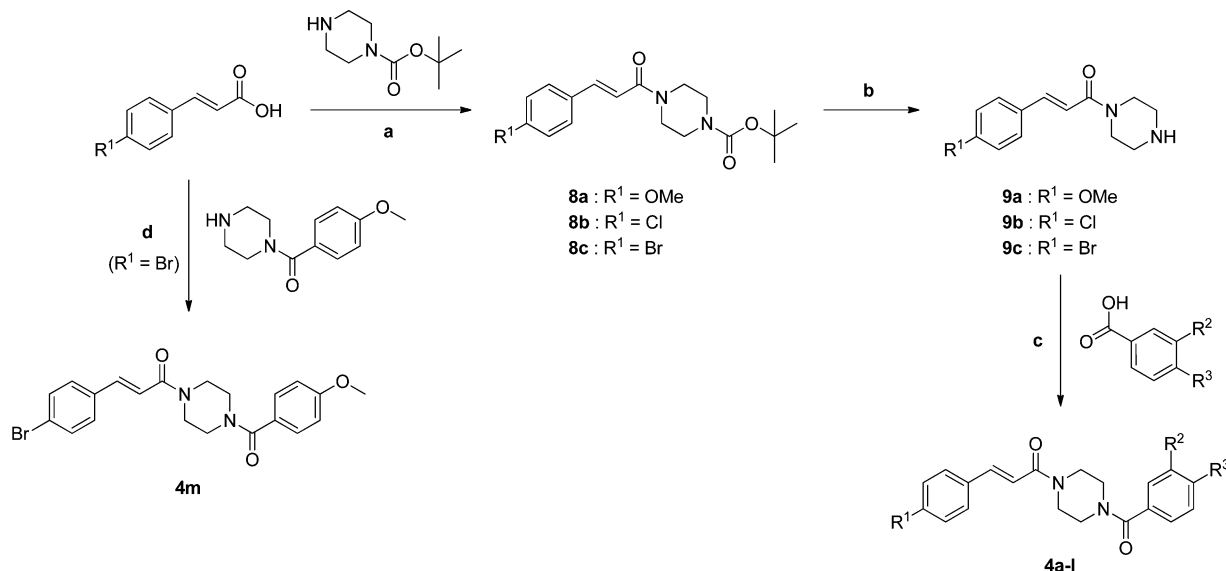
Mouse Liver Microsome Assay. Metabolic stability of compounds was determined in mouse liver microsome assay using the compound depletion approach quantified by LC-MS/MS as previously described.^{24,25} In brief, 30 μ L of compound (10 μ M in 0.1% DMSO/water) was added to 120 μ L of human liver microsomal protein (1.25 mg/mL; male mouse (CD-1) liver microsomes (BD Biosciences)) suspended in phosphate buffer (pH 7.4). Reactions were initiated by the addition of 150 μ L of a cofactor solution containing 2

mM NADPH. At specific reaction time points (0, 5, 20, and 30 min), aliquots (50 μ L) were removed and reactions were terminated by the addition to acetonitrile (100 μ L) containing the analytical internal standards (1 μ M alprenolol and 1.6 μ M chlorzoxazone) and stored at -20 $^{\circ}$ C for at least 1 h to allow complete precipitation of proteins. The samples were then centrifuged, and 20 μ L of the supernatants were analyzed by LC-MS/MS for quantitation of the remaining compound. The percentage of compound remaining, relative to time zero minute incubation, was used to estimate the in vitro elimination-rate constant (k_{met}), which is used to calculate the in vitro metabolic half-life ($t_{1/2}$, min) and intrinsic clearance (CL_{int} , μ L \cdot min⁻¹ \cdot mg⁻¹) rates. In general, compounds with high in vitro CL_{int} (>150 μ L \cdot min⁻¹ \cdot mg⁻¹) are considered to be at high risk for exposure-limiting metabolism in vivo. Compounds with low in vitro CL_{int} (<50 μ L \cdot min⁻¹ \cdot mg⁻¹) are not expected to be at significant risk for exposure-limiting metabolism in vivo.

Pharmacokinetic Analysis. Pharmacokinetic parameters were calculated from blood levels after iv (1 mg \cdot kg⁻¹) and po (3 mg \cdot kg⁻¹) administration to conscious male mice (3 mice/time point; strain, C57BL/6; age, 9–11 weeks; source, Charles River, Iffa Credo, France). Cassette dosing was used with six compounds in maximum. For iv application, compounds were formulated in *N*-methyl-2-pyrrolidone (NMP):plasma (10:90), administration volume 5 mL \cdot kg⁻¹. For po dosing, a compound suspension was formulated in Tween 80:carboxymethylcellulose (CMC05) (0.5:99.5), administration volume 10 mL \cdot kg⁻¹. The animals were housed in groups of three in normal cages with free access to food and tap water throughout the experiment. All animal procedures were approved by the Institutional Animal Care and Use Committee (IACUC) and ethics committee. Sampling time points for iv dosing were at 0.08, 0.5, 1.0, 2.0, 4.0, 8.0, and 24.0 h and for po dosing at 0.25, 0.5, 1.0, 2.0, 4.0, 8.0, and 24.0 h. Then 30 μ L of blood (EDTA sample collection) was mixed with 200 μ L of acetonitrile and centrifuged at 4 $^{\circ}$ C. Then 200 μ L of supernatant were transferred into a microtiter plate, solvent evaporated, and residue dissolved in 60 μ L of methanol and 40 μ L of 0.1% formic acid. An aliquot of each sample was injected into the LC-MS/MS system for analysis.

Compounds. 7 α ,25-OHC (CAS no. 64907-22-8) was purchased from Avanti Polar Lipids Inc. (Alabaster, AL). Compounds 1 and 2 were purchased from Maybridge (UK) and Chembridge (San Diego, CA), respectively.

Synthesis. Compounds 2a–c and 3a–e were prepared as shown in Scheme 1. The common intermediate 6 to both series was easily synthesized in two steps by acylation of the commercially available *tert*-butyl piperazine-1-carboxylate with 2-phenylacetyl chloride under basic conditions to give 5, which was subsequently Boc deprotected

Scheme 2. Synthesis of Compounds 4a–m^a

^aReagents and conditions: (a) Et₃N, HATU, DMF, RT, 2 h, 63%–96%; (b) HCl 4N, dioxane, RT, 16 h, 89%–quant; (c) Et₃N, HATU, DMF, RT, 3 h, 27%–77%; (d) NMM, HATU, DMF, RT, 16 h, 69%.

with TFA. The intermediate **6** was further acylated with chloroacetyl chloride under basic conditions to give **7**, which reacted with appropriate phenolates (generated in situ in the presence of K₂CO₃) under nucleophilic reaction conditions to deliver the final compounds **2a–c** in good yields. Starting from the same intermediate **6**, compounds **3a–e** were obtained in one step by amide coupling reactions with appropriate cinnamic acids, using HATU as a coupling reagent.

A three-step reaction sequence was used for the preparation of compounds **4a–l** as disclosed in Scheme 2. Amide coupling reactions performed on appropriate cinnamic acids with *tert*-butyl piperazine-1-carboxylate, using the same conditions as for the preparation of compounds **3**, gave the intermediates **8a–c**. Boc deprotection with HCl in dioxane delivered the HCl salts **9a–c**, which subsequently reacted with various carboxylic acids under similar amide coupling reaction conditions as described before to give the desired compounds **4a–l**. As a higher amount of our tool compounds **4m** was required to support our biological activities, a specific one-step synthesis was achieved from commercially available building blocks; the coupling of (*E*)-3-(4-bromophenyl)acrylic acid with (4-methoxyphenyl)-piperazine-1-yl)methanone using previously described reaction conditions delivered **4m** in good yields.

Chemistry. All commercial chemicals and solvents are reagent grade and were used without further purification unless otherwise indicated. All reactions were carried out under an inert atmosphere of argon. Reactions were monitored by LC-MS on a Waters 2695 Alliance HT instrument equipped with a Waters 2996 photodiode array detector (PDA MaxPlot detection at 210.0–400.0 nm) and a C-18 column (Sunfire, 4.6 mm × 20 mm, 3.5 μm) eluting with a linear gradient (5–100% acetonitrile in water containing 0.1% TFA) in 4 min with a flow rate of 3 mL/min and at 35 °C. TLC analysis was performed using precoated silica gel Merck 60 F₂₅₄ glass plates, and spots were detected visually under UV irradiation (254 or 366 nm) or after spraying with phosphomolybdic reagent (Aldrich) followed by heating at 100 °C. Flash column chromatography purifications were done using a medium-pressure Combi-Flash Companion (Isco Inc.) instrument with commercial prepacked silica gel cartridges. Reverse phase prep-HPLC purifications were performed using an optimized gradient elution (acetonitrile/water containing 0.1% TFA) with a Waters HPLC prep-system equipped with a UV detector Waters 2487 dual λ absorbance detector, a MS detector Waters Micromass ZQ, and a reverse phase column SunFire Prep, C-18 OBD, 100 mm × 30 mm, 5 μm, or 100 mm × 19 mm, 5 μm. ¹H NMR were measured on a

Bruker Ultrashield 400 (400 MHz) or a 500 MHz DRX Bruker CryoProbe (500 MHz) spectrometer using trimethylsilane as an internal standard. Chemical shifts (δ values) were reported in parts per million (ppm) downfield from tetramethylsilane, and coupling constants (*J*) were given in Hz. LC-MS data were recorded on a Waters 2795 Alliance HT instrument equipped with a Waters 2996 photodiode array detector (PDA MaxPlot detection at 210.0400.0 nm), a Micromass ZQ detector (positive ion electrospray ionization detection), and a C-18 column (Sunfire C18, 4.6 mm × 20 mm, 3.5 μm) eluting with a linear gradient (5–100% acetonitrile in water both containing 0.1% TFA) in 4 min with a flow rate of 3 mL/min at 45 °C. Purity of all the tested compounds was determined by LC-MS and was found to be ≥95% unless otherwise stated.

***tert*-Butyl 4-(2-Phenylacetyl)piperazine-1-carboxylate (5).** To a solution of *tert*-butyl piperazine-1-carboxylate (4.0 g, 21.48 mmol) and pyridine (3.47 mL, 43.0 mmol) in dry CH₂Cl₂ (100 mL) was added dropwise a solution of 2-phenylacetyl chloride (2.98 mL, 22.55 mmol) in CH₂Cl₂ (10 mL) at 0 °C (ice bath). After the addition, the reaction mixture was allowed to warm to RT and was stirred for 1.5 h. The mixture was diluted with CH₂Cl₂ and washed successively with HCl 2N in water (2×) and Na₂CO₃ 2 M in water (2×). The organic layer was dried over Na₂SO₄, filtered, and evaporated to dryness to yield **5** (6.34 g, 20.83 mmol, 97%) as a white solid, which was used in the next step without further purification. LC-MS (ESI): *m/z* 305.3 [M + H]⁺. ¹H NMR (400 MHz, DMSO-*d*₆): 1.40 (s, 9H) 3.20–3.25 (m, 2H) 3.25–3.30 (m, 2H) 3.42–3.49 (m, 4H) 3.73 (s, 2H) 7.20–7.25 (m, 3H) 7.28–7.32 (m, 2H).

2-Phenyl-1-(piperazin-1-yl)ethanone (6). To a solution of **5** (6.34 g, 20.83 mmol) in CH₂Cl₂ (25 mL) was added TFA (24.07 mL, 312.0 mmol) at RT. The mixture was stirred for 30 min and evaporated to dryness. The residue was dissolved in CH₂Cl₂, and the solution was washed with Na₂CO₃ 2 M in water (2×). The organic layer was dried over Na₂SO₄, filtered, and evaporated to dryness to yield **6** (3.4 g, 16.64 mmol, 80%) as a yellow resin, which was used in the next step without further purification. LC-MS (ESI): *m/z* 205.2 [M + H]⁺. ¹H NMR (400 MHz, DMSO-*d*₆): 2.55–2.61 (m, 2H) 2.61–2.67 (m, 2H) 3.38–3.42 (m, 4H) 3.69 (s, 2H) 7.19–7.25 (m, 3H) 7.27–7.33 (m, 2H).

2-Chloro-1-(4-(2-phenylacetyl)piperazin-1-yl)ethanone (7). To a solution of **6** (1.5 g, 7.34 mmol) and Et₃N (2.05 mL, 14.69 mmol) in CH₂Cl₂ (15 mL) was added dropwise chloroacetyl chloride (0.702 mL, 8.81 mmol) at 0 °C (ice bath). After the addition, the reaction mixture was allowed to warm to RT and was stirred for 30 min. The

mixture was diluted with CH_2Cl_2 and washed successively with HCl 2N in water (2 \times), Na_2CO_3 2 M in water (2 \times) and brine. The organic layer was dried over Na_2SO_4 , filtered, and evaporated to dryness. The crude was purified by silica gel column chromatography (gradient elution, 0.5–10% MeOH in CH_2Cl_2) to yield **7** (1.17 g, 4.17 mmol, 57%) as a brownish resin. TLC: R_f = 0.56 ($\text{CH}_2\text{Cl}_2/\text{MeOH}$ 9:1). LC-MS (ESI): m/z 281.2 $[\text{M} + \text{H}]^+$. ^1H NMR (400 MHz, $\text{DMSO}-d_6$): 3.35–3.56 (m, 8H) 3.73–3.79 (m, 2H) 4.40 (s, 2H) 7.20–7.26 (m, 3H) 7.28–7.34 (m, 2H).

2-(4-Chlorophenoxy)-1-(4-(2-phenylacetyl)piperazin-1-yl)ethanone (2a). To a solution of **7** (30 mg, 0.107 mmol) in DMF (0.5 mL) were successively added K_2CO_3 (29.5 mg, 0.214 mmol) and 4-chlorophenol (16.5 mg 0.128 mmol), and the mixture was stirred at RT for 16 h. The reaction mixture was filtered through a Millipore 0.20 μM filter, and the filter cake was washed with DMF (0.5 mL). The filtrate was directly subjected to purification by reverse phase prep-HPLC (Waters system) to yield **2a** (27.6 mg, 0.074 mmol, 69%) as a light-yellow solid. LC-MS (ESI): m/z 373.3 $[\text{M} + \text{H}]^+$. ^1H NMR (400 MHz, $\text{DMSO}-d_6$): 3.35–3.39 (m, 2H) 3.40–3.44 (m, 2H) 3.45–3.57 (m, 4H) 3.76 (d, J = 6.8, 2H) 4.86 (s, 2H) 6.94 (d, J = 8.8, 2H) 7.22–7.26 (m, 3H) 7.29–7.33 (m, 4H).

2-(4-Bromophenoxy)-1-(4-(2-phenylacetyl)piperazin-1-yl)ethanone (2b). Compound **2b** (33 mg, 0.079 mmol, 74%) was synthesized from **7** (30 mg, 0.107 mmol) and 4-bromophenol (22.2 mg 0.128 mmol) as a yellow resin, in a manner similar to **2a**. LC-MS (ESI): m/z 419.2 $[\text{M} + \text{H}]^+$. ^1H NMR (400 MHz, $\text{DMSO}-d_6$): 3.35–3.58 (m, 8H) 3.72–3.79 (m, 2H) 4.85 (s, 2H) 6.90 (d, J = 8.7, 2H) 7.20–7.27 (m, 3H) 7.29–7.36 (m, 2H) 7.44 (d, J = 8.8, 2H).

2-(3,4-Dimethylphenoxy)-1-(4-(2-phenylacetyl)piperazin-1-yl)ethanone (2c). Compound **2c** (34.9 mg, 0.095 mmol, 89%) was synthesized from **7** (30 mg, 0.107 mmol) and 3,4-dimethylphenol (15.7 mg 0.128 mmol) as a white solid, in a manner similar to **2a**. LC-MS (ESI): m/z 367.3 $[\text{M} + \text{H}]^+$. ^1H NMR (400 MHz, $\text{DMSO}-d_6$): 2.13 (s, 3H) 2.17 (s, 3H) 3.35–3.56 (m, 8H) 3.72–3.78 (m, 2H) 4.74 (s, 2H) 6.63 (dd, J = 8.3, 2.2, 1H) 6.73 (br s, 1H) 7.01 (d, J = 8.3 Hz, 1H) 7.20–7.26 (m, 3H) 7.28–7.35 (m, 2H).

(E)-3-(4-Bromophenyl)-1-(4-(2-phenylacetyl)piperazin-1-yl)prop-2-en-1-one (3a). To a solution of **6** (30 mg, 0.147 mmol) in DMF (0.5 mL) were successively added Et_3N (0.041 mL, 0.294 mmol), (*E*)-3-(4-bromophenyl)acrylic acid (33.3 mg, 0.147 mmol), and HATU (67.0 mg, 0.176 mmol) at RT, and the mixture was stirred for 3 h. The reaction mixture was directly subjected to purification by reverse phase prep-HPLC (Waters system) to yield **3a** (31.9 mg, 0.072 mmol, 49%) as a white solid. LC-MS (ESI): m/z 415.2 $[\text{M} + \text{H}]^+$. ^1H NMR (400 MHz, $\text{DMSO}-d_6$): 3.47–3.57 (m, 6H) 3.59–3.65 (m, 1H) 3.66–3.72 (m, 1H) 3.77 (br s, 2H) 7.21–7.27 (m, 3H) 7.27–7.35 (m, 3H) 7.47 (d, J = 15.4, 1H) 7.61 (d, J = 8.4, 2H) 7.70 (d, J = 8.4, 2H).

(E)-1-(4-(2-Phenylacetyl)piperazin-1-yl)-3-(*p*-tolyl)prop-2-en-1-one (3b). Compound **3b** (31.0 mg, 0.089 mmol, 61%) was synthesized from **6** (30 mg, 0.147 mmol) and (*E*)-3-(*p*-tolyl)acrylic acid (23.8 mg 0.147 mmol) as a white solid, in a manner similar to **3a**. LC-MS (ESI): m/z 349.3 $[\text{M} + \text{H}]^+$. ^1H NMR (400 MHz, $\text{DMSO}-d_6$): 2.33 (s, 3H) 3.47–3.58 (m, 6H) 3.59–3.64 (m, 1H) 3.66–3.72 (m, 1H) 3.77 (br s, 2H) 7.16–7.28 (m, 6H) 7.29–7.36 (m, 2H) 7.47 (d, J = 15.4, 1H) 7.61 (d, J = 8.0, 2H).

(E)-3-(4-Methoxyphenyl)-1-(4-(2-phenylacetyl)piperazin-1-yl)prop-2-en-1-one (3c). Compound **3c** (24.8 mg, 0.068 mmol, 48%) was synthesized from **6** (30 mg, 0.147 mmol) and (*E*)-3-(4-methoxyphenyl)acrylic acid (26.2 mg 0.147 mmol) as a white solid, in a manner similar to **3a**. LC-MS (ESI): m/z 365.3 $[\text{M} + \text{H}]^+$. ^1H NMR (400 MHz, $\text{DMSO}-d_6$): 3.48–3.57 (m, 6H) 3.59–3.64 (m, 1H) 3.65–3.71 (m, 1H) 3.77 (br s, 2H) 3.80 (s, 3H) 6.96 (d, J = 8.7, 2H) 7.10 (d, J = 15.4, 1H) 7.20–7.28 (m, 3H) 7.29–7.35 (m, 2H) 7.46 (d, J = 15.4, 1H) 7.67 (d, J = 8.6, 2H).

(E)-3-(3,4-Dichlorophenyl)-1-(4-(2-phenylacetyl)piperazin-1-yl)prop-2-en-1-one (3d). Compound **3d** (50.0 mg, 0.124 mmol, 84%) was synthesized from **6** (30 mg, 0.147 mmol) and (*E*)-3-(3,4-dichlorophenyl)acrylic acid (31.9 mg 0.147 mmol) as a white solid, in a manner similar to **3a**. LC-MS (ESI): m/z 403.3 $[\text{M} + \text{H}]^+$. ^1H NMR (400 MHz, $\text{DMSO}-d_6$): 3.47–3.58 (m, 6H) 3.60–3.66 (m, 1H) 3.67–

3.74 (m, 1H) 3.75–3.82 (m, 2H) 7.21–7.28 (m, 3H) 7.29–7.42 (m, 3H) 7.47 (d, J = 15.2, 1H) 7.64–7.75 (m, 2H) 8.12 (s, 1H).

(E)-3-(3-Fluoro-4-methylphenyl)-1-(4-(2-phenylacetyl)piperazin-1-yl)prop-2-en-1-one (3e). Compound **3e** (45.6 mg, 0.125 mmol, 85%) was synthesized from **6** (30 mg, 0.147 mmol) and (*E*)-3-(3-fluoro-4-methylphenyl)acrylic acid (26.5 mg 0.147 mmol) as a white solid, in a manner similar to **3a**. LC-MS (ESI): m/z 367.4 $[\text{M} + \text{H}]^+$. ^1H NMR (400 MHz, $\text{DMSO}-d_6$): 2.25 (s, 3H) 3.47–3.57 (m, 6H) 3.59–3.65 (m, 1H) 3.67–3.73 (m, 1H) 3.78 (br s, 2H) 7.21–7.35 (m, 7H) 7.40–7.49 (m, 2H) 7.62 (d, J = 11.4, 1H).

(E)-tert-Butyl 4-(3-(4-Methoxyphenyl)acryloyl)piperazine-1-carboxylate (8a). To a solution of *tert*-butyl piperazine-1-carboxylate (6.07 g, 32.6 mmol) in DMF (100 mL) were successively added Et_3N (9.08 mL, 65.2 mmol), (*E*)-3-(4-methoxyphenyl)acrylic acid (6.10 g, 34.2 mmol), and HATU (13.63 g, 35.8 mmol) at RT, and the mixture was stirred for 2 h. The mixture was diluted with Et_2O and washed successively with HCl 2N in water (2 \times) and Na_2CO_3 2 M in water (2 \times). The organic layer was dried over Na_2SO_4 , filtered, and evaporated to dryness to yield **8a** (10.85 g, 31.3 mmol, 96%) as a white solid, which was used in the next step without further purification. LC-MS (ESI): m/z 347.3 $[\text{M} + \text{H}]^+$. ^1H NMR (400 MHz, $\text{DMSO}-d_6$): 1.42 (s, 9H) 3.33–3.39 (m, 4H) 3.50–3.60 (m, 2H) 3.63–3.72 (m, 2H) 3.79 (s, 3H) 6.96 (d, J = 8.8, 2H) 7.10 (d, J = 15.4, 1H) 7.47 (d, J = 15.2, 1H) 7.67 (d, J = 8.8, 2H).

(E)-tert-Butyl 4-(3-(4-Chlorophenyl)acryloyl)piperazine-1-carboxylate (8b). Intermediate **8b** (2.38 g, 6.78 mmol, 63%) was synthesized from *tert*-butyl piperazine-1-carboxylate (2.0 g, 10.74 mmol) and (*E*)-3-(4-chlorophenyl)acrylic acid (1.96 g, 10.74 mmol) as a white solid, in a manner similar to **8a**. LC-MS (ESI): m/z 351.4 $[\text{M} + \text{H}]^+$. ^1H NMR (400 MHz, $\text{DMSO}-d_6$): 1.42 (s, 9H) 3.33–3.39 (m, 4H) 3.52–3.59 (m, 2H), 3.66–3.72 (m, 2H) 7.29 (d, J = 15.4, 1H) 7.43–7.53 (m, 3H) 7.77 (d, J = 8.6, 2H).

(E)-tert-Butyl 4-(3-(4-Bromophenyl)acryloyl)piperazine-1-carboxylate (8c). Intermediate **8c** (3.36 g, 8.50 mmol, 79%) was synthesized from *tert*-butyl piperazine-1-carboxylate (2.0 g, 10.74 mmol) and (*E*)-3-(4-bromophenyl)acrylic acid (2.44 g, 10.74 mmol) as a white solid, in a manner similar to **8a**. LC-MS (ESI): m/z 397.3 $[\text{M} + \text{H}]^+$. ^1H NMR (400 MHz, $\text{DMSO}-d_6$): 1.42 (s, 9H) 3.33–3.42 (m, 4H) 3.47–3.62 (m, 2H) 3.63–3.76 (m, 2H) 7.30 (d, J = 15.4, 1H) 7.47 (d, J = 15.4, 1H) 7.61 (d, J = 8.3, 2H) 7.69 (d, J = 8.3, 2H).

(E)-3-(4-Methoxyphenyl)-1-(piperazin-1-yl)prop-2-en-1-one (9a). To a solution of **8a** (10.85 g, 31.3 mmol) in dioxane (100 mL) was added HCl 4N in dioxane (66 mL, 264 mmol) at RT, and the mixture was stirred for 16 h. The resulting precipitate was filtered, washed with Et_2O , collected, and dried under high vacuum to yield the HCl salt of **9a** (8.88 g, 31.3 mmol, quant) as an off-white solid. LC-MS (ESI): m/z 247.2 $[\text{M} + \text{H}]^+$. ^1H NMR (400 MHz, $\text{DMSO}-d_6$): 3.06–3.17 (m, 4H) 3.80 (s, 3H) 3.81–4.06 (m, 4H) 6.98 (d, J = 8.8, 2H) 7.12 (d, J = 15.4, 1H) 7.50 (d, J = 15.2, 1H) 7.68 (d, J = 8.8, 2H) 9.40–9.48 (m, 1H).

(E)-3-(4-Chlorophenyl)-1-(piperazin-1-yl)prop-2-en-1-one (9b). Intermediate **9b** (1.74 g, 6.06 mmol, 89%) was synthesized from **8b** (2.38 g, 6.78 mmol) as a white solid (HCl salt), in a manner similar to **9a**. LC-MS (ESI): m/z 251.3 $[\text{M} + \text{H}]^+$. ^1H NMR (400 MHz, $\text{DMSO}-d_6$): 3.03–3.22 (m, 4H) 3.76–3.86 (m, 2H) 3.90–4.03 (m, 2H) 7.31 (d, J = 15.4, 1H) 7.44–7.58 (m, 3H) 7.78 (d, J = 8.4, 2H) 9.27–9.48 (m, 2H).

(E)-3-(4-Bromophenyl)-1-(piperazin-1-yl)prop-2-en-1-one (9c). Intermediate **9c** (2.58 g, 7.78 mmol, 92%) was synthesized from **8c** (3.36 g, 8.5 mmol) as a white solid (HCl salt), in a manner similar to **9a**. LC-MS (ESI): m/z 295.2 $[\text{M} + \text{H}]^+$. ^1H NMR (400 MHz, $\text{DMSO}-d_6$): 3.05–3.21 (m, 4H) 3.75–3.84 (m, 2H) 3.89–4.00 (m, 2H) 7.32 (d, J = 15.4, 1H) 7.50 (d, J = 15.3, 1H) 7.62 (d, J = 8.7, 2H) 7.71 (d, J = 8.1, 2H) 9.23–9.41 (m, 2H).

(E)-3-(4-Methoxyphenyl)-1-(4-(3-methylbenzoyl)piperazin-1-yl)prop-2-en-1-one (4a). To a solution of **9a** (34 mg, 0.120 mmol) in DMF (0.5 mL) were successively added Et_3N (0.050 mL, 0.361 mmol), 3-methylbenzoic acid (16.6 mg, 0.120 mmol), and HATU (54.9 mg, 0.144 mmol) at RT, and the mixture was stirred for 3 h. The reaction mixture was directly subjected to purification by reverse phase prep-HPLC (Waters system) to yield **4a** (29.5 mg, 0.081 mmol, 67%)

as a yellow resin. LC-MS (ESI): m/z 365.3 $[M + H]^+$. 1H NMR (400 MHz, DMSO- d_6): 2.35 (s, 3H) 3.49–3.70 (m, 8H) 3.80 (s, 3H) 6.97 (d, $J = 8.6$, 2H) 7.07–7.17 (m, 1H) 7.20–7.26 (m, 2H) 7.27–7.32 (m, 1H) 7.32–7.38 (m, 1H) 7.48 (d, $J = 15.3$, 1H) 7.63–7.71 (m, 2H).

(*E*)-3-(4-Methoxyphenyl)-1-(4-(4-(trifluoromethyl)benzoyl)piperazin-1-yl)prop-2-en-1-one (**4b**). Compound **4b** (17.5 mg, 0.042 mmol, 39%) was synthesized from **9a** (30 mg, 0.106 mmol) and 4-(trifluoromethyl)benzoic acid (21.2 mg 0.110 mmol) as a white solid, in a manner similar to **4a**. LC-MS (ESI): m/z 419.4 $[M + H]^+$. 1H NMR (400 MHz, DMSO- d_6): 3.28–3.36 (m, 2H) 3.55–3.75 (m, 5H) 3.76–3.86 (m, 4H) 6.97 (d, $J = 8.3$, 2H) 7.05–7.22 (m, 1H) 7.48 (d, $J = 15.3$, 1H) 7.62–7.73 (m, 4H) 7.85 (d, $J = 8.0$, 2H).

(*E*)-1-(4-(4-Bromobenzoyl)piperazin-1-yl)-3-(4-methoxyphenyl)prop-2-en-1-one (**4c**). Compound **4c** (31.2 mg, 0.073 mmol, 60%) was synthesized from **9a** (34 mg, 0.120 mmol) and 4-bromobenzoic acid (24.5 mg 0.120 mmol) as a white solid, in a manner similar to **4a**. LC-MS (ESI): m/z 431.2 $[M + H]^+$. 1H NMR (400 MHz, DMSO- d_6): 3.35–3.41 (m, 2H) 3.53–3.74 (m, 5H) 3.75–3.84 (m, 4H) 6.97 (d, $J = 8.7$, 2H) 7.05–7.19 (m, 1H) 7.41 (d, $J = 8.2$, 2H) 7.48 (d, $J = 15.3$, 1H) 7.62–7.73 (m, 4H).

(*E*)-3-(4-Methoxyphenyl)-1-(4-(4-methylbenzoyl)piperazin-1-yl)prop-2-en-1-one (**4d**). Compound **4d** (30.7 mg, 0.084 mmol, 70%) was synthesized from **9a** (34 mg, 0.120 mmol) and 4-methylbenzoic acid (16.6 mg 0.120 mmol) as a white solid, in a manner similar to **4a**. LC-MS (ESI): m/z 365.3 $[M + H]^+$. 1H NMR (400 MHz, DMSO- d_6): 2.36 (s, 3H) 3.35–4.00 (m, 11H) 6.97 (d, $J = 8.6$, 2H) 7.06–7.17 (m, 1H) 7.24–7.30 (m, 2H) 7.31–7.37 (m, 2H) 7.48 (d, $J = 15.3$, 1H) 7.67 (d, $J = 7.7$, 2H).

(*E*)-1-(4-(4-Methoxybenzoyl)piperazin-1-yl)-3-(4-methoxyphenyl)prop-2-en-1-one (**4e**). Compound **4e** (35.2 mg, 0.093 mmol, 77%) was synthesized from **9a** (34 mg, 0.120 mmol) and 4-methoxybenzoic acid (18.5 mg 0.120 mmol) as a white solid, in a manner similar to **4a**. LC-MS (ESI): m/z 381.3 $[M + H]^+$. 1H NMR (400 MHz, DMSO- d_6): 3.47–3.58 (m, 4H) 3.59–3.67 (m, 2H) 3.72–3.78 (m, 2H) 3.80 (s, 3H) 3.81 (s, 3H) 6.97 (d, $J = 8.8$, 2H) 7.01 (d, $J = 8.8$, 2H) 7.12 (d, $J = 15.2$, 1H) 7.42 (d, $J = 8.8$, 2H) 7.49 (d, $J = 15.4$, 1H) 7.67 (d, $J = 8.6$, 2H).

(*E*)-1-(4-(4-(Dimethylamino)benzoyl)piperazin-1-yl)-3-(4-methoxyphenyl)prop-2-en-1-one (**4f**). Compound **4f** (15.5 mg, 0.039 mmol, 37%) was synthesized from **9a** (30 mg, 0.106 mmol) and 4-(dimethylamino)benzoic acid (18.4 mg 0.110 mmol) as a white solid, in a manner similar to **4a**. LC-MS (ESI): m/z 394.4 $[M + H]^+$. 1H NMR (400 MHz, DMSO- d_6): 2.96 (s, 6H) 3.48–3.66 (m, 6H) 3.70–3.78 (m, 2H) 3.80 (s, 3H) 6.73 (d, $J = 8.7$, 2H) 6.97 (d, $J = 8.6$, 2H) 7.14 (d, $J = 15.4$, 1H) 7.32 (d, $J = 8.7$, 2H) 7.48 (d, $J = 15.3$, 1H) 7.67 (d, $J = 8.6$, 2H).

(*E*)-Methyl 4-(4-(3-(4-Methoxyphenyl)acryloyl)piperazine-1-carbonyl)benzoate (**4g**). Compound **4g** (11.8 mg, 0.029 mmol, 27%) was synthesized from **9a** (30 mg, 0.106 mmol) and 4-(methoxycarbonyl)benzoic acid (20.1 mg 0.110 mmol) as a white solid, in a manner similar to **4a**. LC-MS (ESI): m/z 409.4 $[M + H]^+$. 1H NMR (400 MHz, DMSO- d_6): 3.52–3.84 (m, 8H) 3.79 (s, 3H) 3.89 (s, 3H) 6.97 (d, $J = 8.3$, 2H) 7.04–7.21 (m, 1H) 7.48 (d, $J = 15.4$, 1H) 7.59 (d, $J = 8.1$, 2H) 7.63–7.73 (m, 2H) 8.04 (d, $J = 8.1$, 2H).

(*E*)-1-(4-(2,3-Dihydrobenzofuran-5-carbonyl)piperazin-1-yl)-3-(4-methoxyphenyl)prop-2-en-1-one (**4h**). Compound **4h** (14.5 mg, 0.037 mmol, 35%) was synthesized from **9a** (30 mg, 0.106 mmol) and 2,3-dihydrobenzofuran-5-carboxylic acid (18.3 mg 0.110 mmol) as a white solid, in a manner similar to **4a**. LC-MS (ESI): m/z 393.4 $[M + H]^+$. 1H NMR (400 MHz, DMSO- d_6): 3.21 (t, $J = 8.8$, 2H) 3.46–3.58 (m, 4H) 3.58–3.66 (m, 2H) 3.71–3.78 (m, 2H) 3.80 (s, 3H) 4.58 (t, $J = 8.7$, 2H) 6.81 (d, $J = 8.2$, 1H) 6.97 (d, $J = 8.7$, 2H) 7.13 (d, $J = 15.4$, 1H) 7.21 (d, $J = 8.1$, 1H) 7.34 (s, 1H) 7.48 (d, $J = 15.4$, 1H) 7.67 (d, $J = 8.6$, 2H).

(*E*)-1-(4-(4-Chloro-3-methylbenzoyl)piperazin-1-yl)-3-(4-methoxyphenyl)prop-2-en-1-one (**4i**). Compound **4i** (23.0 mg, 0.058 mmol, 54%) was synthesized from **9a** (30 mg, 0.106 mmol) and 4-chloro-3-methylbenzoic acid (19.0 mg 0.110 mmol) as a white solid, in a manner similar to **4a**. LC-MS (ESI): m/z 399.4 $[M + H]^+$. 1H NMR (400 MHz, DMSO- d_6): 2.37 (s, 3H) 3.35–3.44 (m, 2H) 3.52–3.78

(m, 6H) 3.80 (s, 3H) 6.97 (d, $J = 8.6$, 2H) 7.06–7.20 (m, 1H) 7.29 (d, $J = 8.0$, 1H) 7.42–7.54 (m, 3H) 7.67 (d, $J = 7.6$, 2H).

(*E*)-1-(4-(3,4-Dimethylbenzoyl)piperazin-1-yl)-3-(4-methoxyphenyl)prop-2-en-1-one (**4j**). Compound **4j** (22.1 mg, 0.058 mmol, 55%) was synthesized from **9a** (30 mg, 0.106 mmol) and 3,4-dimethylbenzoic acid (16.7 mg 0.110 mmol) as a white solid, in a manner similar to **4a**. LC-MS (ESI): m/z 379.5 $[M + H]^+$. 1H NMR (400 MHz, DMSO- d_6): 2.26 (s, 6H) 3.36–3.78 (m, 8H) 3.79 (s, 3H) 6.97 (d, $J = 8.6$, 2H) 7.06–7.19 (m, 2H) 7.19–7.25 (m, 2H) 7.48 (d, $J = 15.3$, 1H) 7.67 (d, $J = 8.0$, 2H).

(*E*)-3-(4-Chlorophenyl)-1-(4-(2,3-dihydrobenzofuran-6-carbonyl)piperazin-1-yl)prop-2-en-1-one (**4k**). Compound **4k** (29.2 mg, 0.074 mmol, 40%) was synthesized from **9b** (52.6 mg, 0.183 mmol) and 2,3-dihydrobenzofuran-5-carboxylic acid (30.0 mg 0.183 mmol) as a white solid, in a manner similar to **4a**. LC-MS (ESI): m/z 397.3 $[M + H]^+$. 1H NMR (400 MHz, DMSO- d_6): 3.22 (t, $J = 8.7$, 2H) 3.47–3.67 (m, 6H) 3.73–3.82 (m, 2H) 4.59 (t, $J = 8.7$, 2H) 6.81 (d, $J = 8.2$, 1H) 7.21 (d, $J = 8.2$, 1H) 7.27–7.37 (m, 2H) 7.45–7.55 (m, 3H) 7.77 (d, $J = 8.4$, 2H).

(*E*)-3-(4-Bromophenyl)-1-(4-(2,3-dihydrobenzofuran-6-carbonyl)piperazin-1-yl)prop-2-en-1-one (**4l**). Compound **4l** (41.9 mg, 0.095 mmol, 52%) was synthesized from **9c** (60.7 mg, 0.183 mmol) and 2,3-dihydrobenzofuran-5-carboxylic acid (30.0 mg 0.183 mmol) as a white solid, in a manner similar to **4a**. LC-MS (ESI): m/z 443.2 $[M + H]^+$. 1H NMR (400 MHz, DMSO- d_6): 3.21 (t, $J = 8.7$, 2H) 3.48–3.58 (m, 4H) 3.58–3.65 (m, 2H) 3.73–3.80 (m, 2H) 4.58 (t, $J = 8.7$, 2H) 6.81 (d, $J = 8.3$, 1H) 7.21 (dd, $J = 8.2$, 1.6, 1H) 7.28–7.36 (m, 2H) 7.49 (d, $J = 15.4$, 1H) 7.60–7.63 (m, 2H) 7.68–7.71 (m, 2H).

(*E*)-3-(4-Bromophenyl)-1-(4-(4-methoxybenzoyl)piperazin-1-yl)prop-2-en-1-one (**4m**). To a solution of (4-methoxyphenyl)-(piperazin-1-yl)methanone (0.970 g, 4.40 mmol) in DMF (17 mL) were successively added *N*-methylmorpholine (2.4 mL, 22.02 mmol), (*E*)-3-(4-bromophenyl)acrylic acid (1.0 g, 4.40 mmol), and HATU (1.84 g, 4.84 mmol) at RT, and the mixture was stirred for 16 h. The mixture was diluted with AcOEt, and the solution was washed successively with HCl 2N in water and Na₂CO₃ 2 M in water and brine. The organic layer was dried over Na₂SO₄, filtered, and evaporated to dryness. The resulting crude residue was purified by silica gel column chromatography (gradient elution, 0.5–10% MeOH in CH₂Cl₂) to give the title compound as a light-yellow solid. The solid was recrystallized in AcOEt/MeOH (1:1, 100 mL) to yield **4m** (1.30 g, 3.03 mmol, 69%) as a colorless crystalline solid. LC-MS (ESI): m/z 431.2 $[M + H]^+$. 1H NMR (400 MHz, DMSO- d_6): 3.47–3.59 (m, 3H) 3.59–3.66 (m, 2H) 3.73–3.79 (m, 2H) 3.81 (s, 3H) 7.00 (d, $J = 8.6$, 2H) 7.32 (d, $J = 15.4$, 1H) 7.42 (d, $J = 8.6$, 2H) 7.49 (d, $J = 15.4$, 1H) 7.59–7.64 (m, 2H) 7.67–7.73 (m, 2H).

■ ASSOCIATED CONTENT

Ⓢ Supporting Information

Dose–response curves for key compounds measuring release of intracellular calcium in CHO cells expressing human EB12 receptor. [³H] 7 α ,25-OHC radioligand binding data for all compounds at the human EB12 receptor. This material is available free of charge via the Internet at <http://pubs.acs.org>.

■ AUTHOR INFORMATION

Corresponding Author

*Phone: +41 79 5500941. Fax: +41 61 3246105. E-mail: andreas.sailer@novartis.com. Address: Developmental & Molecular Pathways, Novartis Institutes for BioMedical Research, Forum 1, Novartis Campus, WSJ-355.4025.8 4002 Basel, Switzerland.

Present Addresses

#For D.G.N.: Organovo, Inc., 6275 Nancy Ridge Drive, San Diego, California, 92121, United States.

∇For Y.A.C.: NGM Biopharmaceuticals, Inc., 630 Gateway Blvd., South San Francisco, California, 94080, United States.

Notes

The authors declare the following competing financial interest(s): All authors, except for M. M. Rosenkilde, are current or previous employees of Novartis and some of them do hold stock or stock options in their company.

ACKNOWLEDGMENTS

We thank Emilie Joly, Pierre Nimsgern, and Inger Smith Simonson for their excellent technical assistance. We are grateful to Drs. Günther Scheel, Shin Numao, and John Priestley for supporting activities closely connected to this project.

ABBREVIATIONS USED

7 α ,25-OHC, 7 α ,25-dihydroxycholesterol; RHS, right-hand side; LHS, left-hand side; EBI2, Epstein–Barr virus-induced gene 2; Cl_{int} , intrinsic clearance; SD, standard deviation; CHO, Chinese hamster ovary; SPA, scintillation proximity assay; WGA, wheat germ agglutinin; PVT, polyvinyltoluene; V_{ss} , apparent volume of distribution at steady state; C_{max} , maximal blood concentration after po administration; T_{max} , time of peak blood concentration after po administration; HATU, (1-[bis-(dimethylamino)methylene]-1H-1,2,3-triazolo[4,5-b]-pyridinium3-oxide hexafluorophosphate)

REFERENCES

- (1) Hannedouche, S.; Zhang, J.; Yi, T.; Shen, W.; Nguyen, D.; Pereira, J. P.; Guerini, D.; Baumgarten, B. U.; Roggo, S.; Wen, B.; Knochenmuss, R.; Noel, S.; Gessier, F.; Kelly, L. M.; Vanek, M.; Laurent, S.; Preuss, I.; Miault, C.; Christen, L.; Karuna, R.; Li, W.; Koo, D. I.; Suply, T.; Schmedt, C.; Peters, E. C.; Falchetto, R.; Katopodis, A.; Spanka, C.; Roy, M. O.; Detheux, M.; Chen, Y. A.; Schultz, P. G.; Cho, C. Y.; Seuwen, K.; Cyster, J. G.; Sailer, A. W. Oxysterols direct immune cell migration via EBI2. *Nature* **2011**, *475*, 524–527.
- (2) Liu, C.; Yang, X. V.; Wu, J.; Kuei, C.; Mani, N. S.; Zhang, L.; Yu, J.; Sutton, S. W.; Qin, N.; Banie, H.; Karlsson, L.; Sun, S.; Lovenberg, T. W. Oxysterols direct B-cell migration through EBI2. *Nature* **2011**, *475*, 519–523.
- (3) Rosenkilde, M. M.; Benned-Jensen, T.; Andersen, H.; Holst, P. J.; Kledal, T. N.; Luttichau, H. R.; Larsen, J. K.; Christensen, J. P.; Schwartz, T. W. Molecular pharmacological phenotyping of EBI2. An orphan seven-transmembrane receptor with constitutive activity. *J. Biol. Chem.* **2006**, *281*, 13199–13208.
- (4) Heinig, M.; Petretto, E.; Wallace, C.; Bottolo, L.; Rotival, M.; Lu, H.; Li, Y.; Sarwar, R.; Langley, S. R.; Bauerfeind, A.; Hummel, O.; Lee, Y. A.; Paskas, S.; Rintisch, C.; Saar, K.; Cooper, J.; Buchan, R.; Gray, E. E.; Cyster, J. G.; Erdmann, J.; Hengstenberg, C.; Maouche, S.; Ouwehand, W. H.; Rice, C. M.; Samani, N. J.; Schunkert, H.; Goodall, A. H.; Schulz, H.; Roider, H. G.; Vingron, M.; Blankenberg, S.; Munzel, T.; Zeller, T.; Szymczak, S.; Ziegler, A.; Tired, L.; Smyth, D. J.; Pravenec, M.; Aitman, T. J.; Cambien, F.; Clayton, D.; Todd, J. A.; Hubner, N.; Cook, S. A. A trans-acting locus regulates an anti-viral expression network and type 1 diabetes risk. *Nature* **2010**, *467*, 460–464.
- (5) Gill, S.; Chow, R.; Brown, A. J. Sterol regulators of cholesterol homeostasis and beyond: the oxysterol hypothesis revisited and revised. *Prog. Lipid Res.* **2008**, *47*, 391–404.
- (6) Janowski, B. A.; Shan, B.; Russell, D. W. The hypocholesterolemic agent LY295427 reverses suppression of sterol regulatory element-binding protein processing mediated by oxysterols. *J. Biol. Chem.* **2001**, *276*, 45408–45416.
- (7) Janowski, B. A.; Grogan, M. J.; Jones, S. A.; Wisely, G. B.; Kliewer, S. A.; Corey, E. J.; Mangelsdorf, D. J. Structural requirements of ligands for the oxysterol liver X receptors LXRalpha and LXRbeta. *Proc. Natl. Acad. Sci. U. S. A.* **1999**, *96*, 266–271.
- (8) Wang, Y.; Kumar, N.; Crumbley, C.; Griffin, P. R.; Burris, T. P. A second class of nuclear receptors for oxysterols: regulation of

RORalpha and RORgamma activity by 24S-hydroxycholesterol (cerebrosterol). *Biochim. Biophys. Acta* **2010**, *1801*, 917–923.

- (9) Kallen, J.; Schlaeppli, J. M.; Bitsch, F.; Delhon, I.; Fournier, B. Crystal structure of the human RORalpha ligand binding domain in complex with cholesterol sulfate at 2.2 Å. *J. Biol. Chem.* **2004**, *279*, 14033–14038.

- (10) Kallen, J. A.; Schlaeppli, J. M.; Bitsch, F.; Geisse, S.; Geiser, M.; Delhon, I.; Fournier, B. X-ray structure of the hRORalpha LBD at 1.63 Å: structural and functional data that cholesterol or a cholesterol derivative is the natural ligand of RORalpha. *Structure* **2002**, *10*, 1697–1707.

- (11) Raychaudhuri, S.; Prinz, W. A. The diverse functions of oxysterol-binding proteins. *Annu. Rev. Cell Dev. Biol.* **2010**, *26*, 157–177.

- (12) Ohgane, K.; Karaki, F.; Dodo, K.; Hashimoto, Y. Discovery of oxysterol-derived pharmacological chaperones for NPC1: implication for the existence of second sterol-binding site. *Chem. Biol.* **2013**, *20*, 391–402.

- (13) Dwyer, J. R.; Sever, N.; Carlson, M.; Nelson, S. F.; Beachy, P. A.; Parhami, F. Oxysterols are novel activators of the hedgehog signaling pathway in pluripotent mesenchymal cells. *J. Biol. Chem.* **2007**, *282*, 8959–8968.

- (14) Nachtergaele, S.; Mydock, L. K.; Krishnan, K.; Rammohan, J.; Schlesinger, P. H.; Covey, D. F.; Rohatgi, R. Oxysterols are allosteric activators of the oncoprotein Smoothened. *Nature Chem. Biol.* **2012**, *8*, 211–220.

- (15) Nedelcu, D.; Liu, J.; Xu, Y.; Jao, C.; Salic, A. Oxysterol binding to the extracellular domain of Smoothened in Hedgehog signaling. *Nature Chem. Biol.* **2013**, *9*, 557–564.

- (16) Yi, T.; Wang, X.; Kelly, L. M.; An, J.; Xu, Y.; Sailer, A. W.; Gustafsson, J. A.; Russell, D. W.; Cyster, J. G. Oxysterol gradient generation by lymphoid stromal cells guides activated B cell movement during humoral responses. *Immunity* **2012**, *37*, 535–548.

- (17) Benned-Jensen, T.; Smethurst, C.; Holst, P. J.; Page, K. R.; Sauls, H.; Sivertsen, B.; Schwartz, T. W.; Blanchard, A.; Jepras, R.; Rosenkilde, M. M. Ligand modulation of the Epstein–Barr virus-induced seven-transmembrane receptor EBI2: identification of a potent and efficacious inverse agonist. *J. Biol. Chem.* **2011**, *286*, 29292–29302.

- (18) Benned-Jensen, T.; Madsen, C. M.; Arfelt, K. N.; Smethurst, C.; Blanchard, A.; Jepras, R.; Rosenkilde, M. M. Small molecule antagonism of oxysterol-induced Epstein–Barr virus induced gene 2 (EBI2) activation. *FEBS Open Bio* **2013**, *3*, 156–160.

- (19) Hammer, M. M.; Wehrman, T. S.; Blau, H. M. A novel enzyme complementation-based assay for monitoring G-protein-coupled receptor internalization. *FASEB J.* **2007**, *21*, 3827–3834.

- (20) Yin, H.; Chu, A.; Li, W.; Wang, B.; Shelton, F.; Otero, F.; Nguyen, D. G.; Caldwell, J. S.; Chen, Y. A. Lipid G protein-coupled receptor ligand identification using beta-arrestin PathHunter assay. *J. Biol. Chem.* **2009**, *284*, 12328–12338.

- (21) Eibinger, G.; Fauler, G.; Bernhart, E.; Frank, S.; Hammer, A.; Wintersperger, A.; Eder, H.; Heinemann, A.; Mischel, P. S.; Malle, E.; Sattler, W. On the role of 25-hydroxycholesterol synthesis by glioblastoma cell lines. Implications for chemotactic monocyte recruitment. *Exp. Cell Res.* **2013**, *319*, 1828–1838.

- (22) Brown, A. J.; Jessup, W. Oxysterols and atherosclerosis. *Atherosclerosis* **1999**, *142*, 1–28.

- (23) Moore, K. J.; Tabas, I. Macrophages in the pathogenesis of atherosclerosis. *Cell* **2011**, *145*, 341–355.

- (24) Benned-Jensen, T.; Norn, C.; Laurent, S.; Madsen, C. M.; Larsen, H. M.; Arfelt, K. N.; Wolf, R. M.; Frimurer, T.; Sailer, A. W.; Rosenkilde, M. M. Molecular characterization of oxysterol binding to the Epstein–Barr virus-induced gene 2 (GPR183). *J. Biol. Chem.* **2012**, *287*, 35470–35483.

- (25) Trunzer, M.; Faller, B.; Zimmerlin, A. Metabolic soft spot identification and compound optimization in early discovery phases using MetaSite and LC-MS/MS validation. *J. Med. Chem.* **2009**, *52*, 329–335.